On the Existence of Time Delay for Rotating Beam with Proportional–Derivative Controller

K RAVI, P SOMA SEKHAR, C SUBBI REDDY
ASSISTANT PROFESSOR [1,2,3]
kollamadaravi111@gmail.com, Paletisomasekhar@gmail.com, cheemalasubbireddy@gmail.com
Department of Mathematics, Sri Venkateswara Institute of Technology,
N.H 44, Hampapuram, Rapthadu, Anantapuramu, Andhra Pradesh 515722

Abstract

A mathematical model of a revolving beam at different speeds is examined. The approximation solution of the system behaviour in the resonance situation is studied through the application of the multiple time scales method to the nonlinear system of differential equations. We looked at the system when a proportional-derivative (PD) controller was used to apply delayed control to displacement and velocity. Using the Routh-Huriwitz method, the consistency of the steady state solution in the near-resonance scenario is evaluated and examined. We identify and examine the factors affecting the steady state solution of the different parameters. The MATLAB software package is used to obtain simulation effects. To demonstrate and contrast controller effects at different system settings, different response curves are used.

Keywords: Active feedback controller, time delay, various time scales approach, and nonlinear dynamical system.

Introduction

Unwanted occurrences in dynamical and structural structures are always disruptions and complicated instability. For many reasons, including geometric nonlinearities, nonlinear powers of excitation, and the nonlinear characteristics of materials, these systems are subject to nonlinear vibrations. A lot of time, money, and effort goes into reducing the oscillations and vibrations in these systems to prolong their lifespan and guard against damage or failure.

This issue, which has an impact on industry, frugality, and equipment, has drawn the attention and efforts of numerous academics and scientists. Thomas et al. [1] address the high amplitude nonlinear vibration activity of a revolving cantilever beam, with applications for turbo-propeller blades and turbo equipment. We looked into how the rotation speed affected the beam's nonlinear vibrations, specifically how its resonances behaved in terms of hardness and softness and whether or not large amplitude jump phenomena occurred. Zhang et al. [2] looked into a new dynamic model of a rotating flexible beam based on the absolute nodal coordinate formulation with a condensed mass placed at any spot. They discovered that the normal frequencies and the mode shapes are affected by the condensed mass's magnitude and direction. Rezaei et al. [3] performed an aeroelastic analysis of a spinning wind turbine blade by taking into account the impact of geometrical nonlinearities related to significant blade deflection produced during wind turbine operation. They presented an aerodynamic model based on the strip theory by utilising the ideas of quasi-steady and unstable airfoil aerodynamics. The findings demonstrated geometric nonlinearity,

had a notable effect, particularly for bigger structural deformations. In [4], the impact of rotation velocity on nonlinear resonances is examined, and in [5], the von Kármán model is solved through the application of the multi-scale perturbation approach. Using nonlinear beam models like axial inertia and nonlinear curvature, nonlinear resonances are simulated using a one-mode Galerkin expansion. Additionally, nonlinear resonance curves are generated using a fully numerical method (harmonic balance combined with an asymptotic numerical technique), based on a Galerkin discretization with Legendre polynomials and a continuity process. Kim and Chung proposed a nonlinear model for a more thorough and efficient dynamic analysis of a rotating cantilever beam with elastic deformation specified by partial integro-differential equations with non-Cartesian deformation variables. They demonstrated how the suggested model not only offered good numerical efficiency and precision, but also successfully overcame the limitations caused by the Cartesian variables of an earlier conventional nonlinear model. Latalski [7] proposed the dynamics of a construction made up of a thin-walled composite beam with an embedded active portion and a rotating rigid hub.

They examined the natural mode forms and the spatial distribution of the electrical field based on

the device rotation velocity and the laminae fibre orientation angle. Kandil, H. El-Gohary [8] investigated the effects of time delay on its output to reduce the oscillations of a spinning beam at various speeds using a proportional derivative (PD) controller. Despite the dual system's linearly coupled vibrational modes, only one of the modes receives controller input; the other coupled mode follows the active mode. They controlled the device in the worst resonance conditions, which were confirmed quantitatively. Yao et al. [9,10] deduced the governing equations for the beam by applying the theory and isotropic constitutive law of Hamilton. They investigated the dynamics of high temperature and supersonic gas flow at various speeds. With the use of macrofiber composite (MFC) actuators and polyvinylidene fluoride (PVDF) sensors, Choi et al. [11,12] demonstrated how to achieve an active damping effect using a negative velocity feedback control technique. MFC is a type of piezoelectric material that is composite. Adequate vibration suppression efficiency would consequently be achieved by the necessary configuration and distribution scale of the sensor/actuator combination.

Joy Mondal and S. Chatterjee [13] suggested that a velocity feedback based nonlinear resonant controller would be effective in controlling a nonlinear beam's forced and free self-excited vibration. The velocity signal from the sensor is sent through a second-order filter, and the nonlinear function of the derivative of the filter vector is used to calculate the control force. For vibration investigations of rotating versatile beams with improved active constrained layer damping (EACLD) treatment that is partially shielded, Liang Li et al. [14] have created a new hierarchical model. By representing the edge element of the EACLD patch as an analogous spring with associated point mass, the mass effect of the two additional edge components is included. The discrete rigid-flexible coupled dynamic equations of hub-beam systems with EACLD treatment in the open-loop and closed-loop scenarios are obtained using the assumed mode approach and Lagrange's equations.

According to Boumediène and Smaoui [15], the beam is supposed to be non-uniform and clamped at its left end to the disk's core, where torque control takes place. At the right end, however, is where a memory boundary control is located. First, the conventional torque control is proposed, and then the boundary control is designed based on the dynamic properties of the input and a unique kind of memory phenomena. A new operational modal analysis (OMA) method for a rotating structure was developed by L.F. Lyu and W.D. Zhu [16]. It was based on an image processing technique, a lifting way of data processing, and a rigorous rotating beam vibration theory. The rotating structure's real-time location was ascertained through image processing, which allowed the TCSLDV system to track a time-varying scan direction on the rotating structure. They then developed a novel tracking continuously scanning laser Doppler vibrometer (TCSLDV) method to monitor and scan a rotating structure.

In order to lessen oscillations and improve efficiency, the PID control with time delay control is used to the system of rotating beam at different speeds depicted in Fig. 1a [8,9,10] that is subjected to external and parametric force. As illustrated in Fig. 1b, MFC sensors are positioned across the blade's bottom surface to monitor displacements of the blade cross section. As seen in Fig. 1c, the measured signals will be returned to the computer for analysis and computation of the proper control signal. A control loop feedback mechanism shown in Fig. 2 continuously calculates an error value e(t) as the difference between a desired setpoint (SP) and a measured process variable (PV), and once the control signal has been calculated, it is passed through a conditioning circuit and applied to the embedded MFC actuators that are distributed over the top of the blade to modify the blade position and reduce its vibration.

makes adjustments using derivative, integral, and proportional terms (abbreviated P, I, and D, respectively).Using the multiple time scales perturbation technique (MSPT), the response equation was displayed and an approximate solution was obtained. The phase plane and the frequency response equation are both used to examine the system's stability in the primary and principal parametric resonance cases. The nonlinear dynamic system's reaction and the impact of various factors are examined by numerical means.

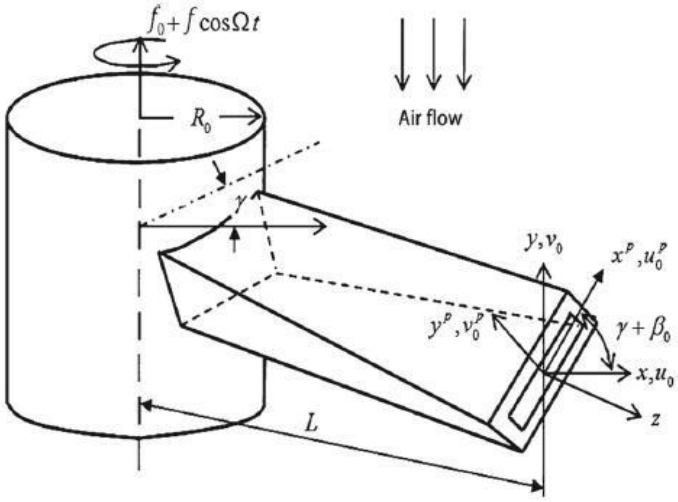

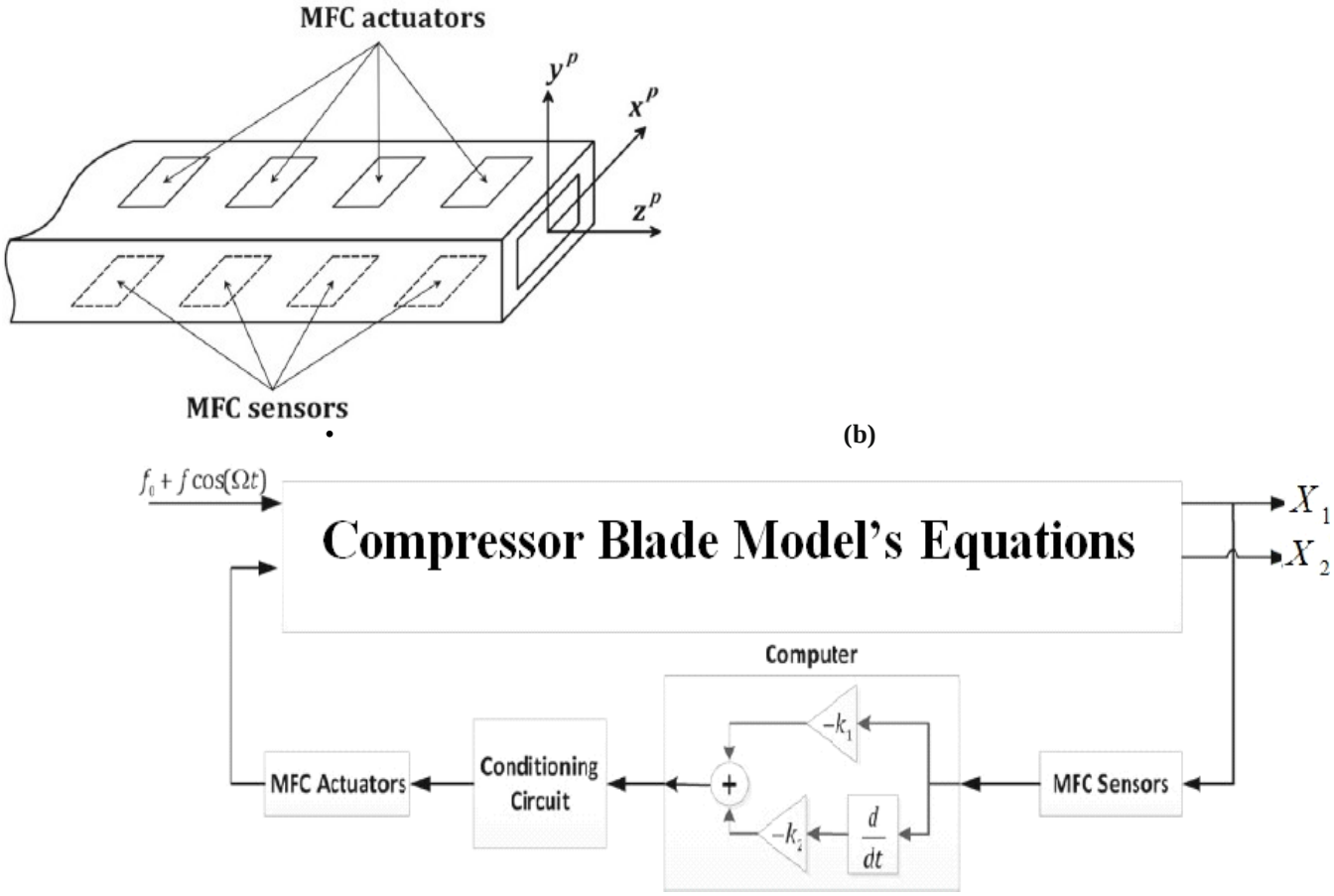

Fig. 1. Rotating compressor blade model, (a) thin-walled pre-twisted blade, (b) sensors and actuators distribution and (c) block diagram of control process

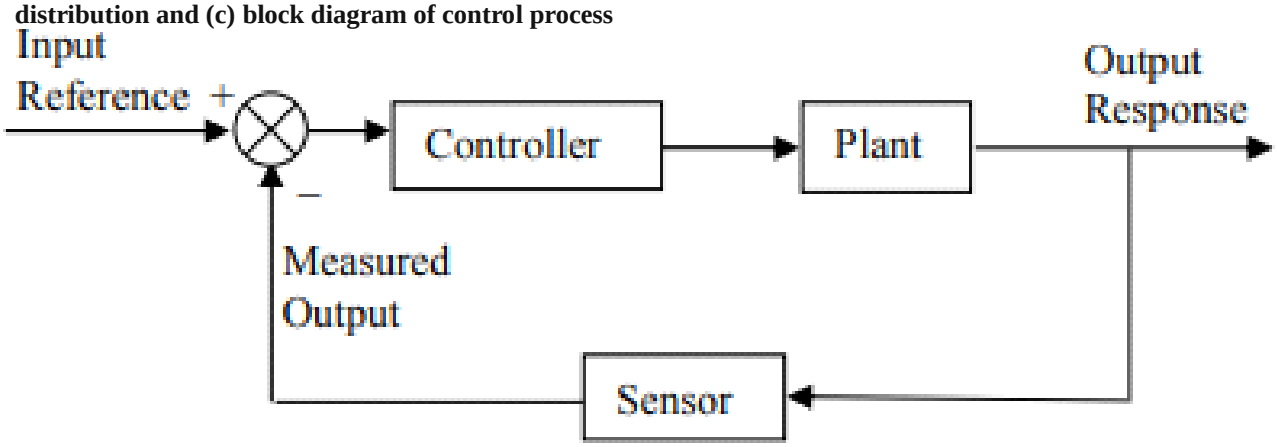

Fig. 2 A closed loop system controller

• System Model and Mathematical Analysis

The equations of motion for the rotating beam shown in Fig. 1 is introduced by Bekhoucha [5] and Yao et al. [9, 10] by applying the Hamilton's principle as:

$$\int_0^t (\delta K - \delta U + \delta W)\, dt \,' \qquad (1)$$

where K denote the kinetic energy, U the strain energy, and W is the virtual work of external forces, t denotes time, and δ is the variation operator. By calculating the variation in kinetic, strain energy, and the virtual work of non-conservative external forces (given in Appendix), and substituting Equation (1), then the governing equations of the nonlinear vibration system for the rotating beam are as the following:

$$\ddot{u} - \Omega^2\left[u + R(z)u' + R'(z)u'\right] + \alpha\,\Delta T\,u' - \left[a_1(z)v' - a_3(z)u'\right]' = u'\left[u'u' + v'v'\right] + u'\left[\frac{1}{2}(u')^2 + \frac{1}{2}(v')^2\right] - \Omega(R_o + z) + p_x,$$

(2)

$$\ddot{v} - \Omega^2\left[R(z)v' + R'(z)v'\right] + \alpha\,\Delta T\,v' - \left[a_2(z)u' - a_3(z)v'\right]' = v'\left[u'u' + v'v'\right] + v'\left[\frac{1}{2}(u')^2 + \frac{1}{2}(v')^2\right] + p_y,$$

where u, v are the translations along the x, and y axes,

p_x , p_y

are the external forces per unit axial length in

the x and the y direction. The values of

p_x , p_y and the variables $a_i(z), i = 1,2,3,$ are given in Appendix.

The dots and primes, respectively, represent partial differentiation with respect to t and z, *R(X,Y,Z)* is the vector function of a point *M(X,Y,Z)* of the deformed thin wall beam, and given by $R(X, Y, Z) = (X + u)i + (Y + v)\,j + Z\,k + R_o$. Applying Galerkin's approach [17] on system (2),

the

horizontal and vertical displacements u ,v have been approximated to the modes X_1 , X_2 respectively tohave the dimensionless two degree of freedom non-linear rotating beam system in the form:

$$\ddot{X} + 2\mu\dot{X} + \omega^2 X + \beta X + \beta X X^2 + \beta X^3 = 2f f \beta X$$

$\cos(\Omega t)$

1 1 1 1 13 2 11 2 5 1 2 5 1 o 14 1

$$+f\ ^2\beta\ \ X\ \ \cos^2(\Omega t)+f\ \beta\ \ \Omega\sin(\Omega t)-k\ X\ \ (t-\tau)-k\ X\ \ (t-\tau),$$

(3a)

14 1 16 1 1 2 1

$$X\ \ +2\mu\ X\ \ +\omega^2 X\ \ +\beta\ \ X\ \ +$$

$$\beta\ \ X\ \ +\beta\ X\ \ X^{\,2}+\beta\ X^{\,3}=2f\ \ f\ \beta\ \ X$$

$\cos(\Omega t)$

2 2 2 2 22 1 21 1 5 2 1 5 2 o 24 2

$+f\ ^2\beta$

$_{24}X_{\,2}$

$\cos^2(\Omega t),$

(3b)

where all system parameters are defined before.

Scaling the previous parameters as:

$$\beta_{11}=\varepsilon\hat{\beta}\ ,\beta\ \ =\varepsilon\hat{\beta}\ ,\beta\ \ =\varepsilon\hat{\beta}\ ,\beta\ \ =\varepsilon\hat{\beta}\ ,\beta\ \ =\varepsilon\hat{\beta}\ ,\beta\ \ =\varepsilon\hat{\beta}\ ,\beta\ \ =\varepsilon\hat{\beta}\ ,\beta\ =\varepsilon\hat{\beta}\ ,$$

11 13 13 14 14 16 16 21 21 22 22 24 24 5 5

(4)

$$k_1=\varepsilon\hat{k}\ ,k\ =\varepsilon\hat{k}\ ,\mu\ =\varepsilon\hat{\mu}\ ,\mu\ =\varepsilon\hat{\mu}\ .$$

1 2 2 1 1 2 2

Applying multiple time scales method [18], an asymptotic expansion is sought as:

1 o 1 10 o 1 11 o 1

$$X\ (T\ ,T\ ,\varepsilon)=X\ \ (T\ ,T\ )+\varepsilon X\ \ (T\ ,T\ )+O(\varepsilon^{2}),$$

2 o 1 20 o 1 21 o 1

$$X\ (T\ ,T\ ,\varepsilon)=X\ \ (T\ ,T\ )+\varepsilon X\ \ (T\ ,T\ )+O(\varepsilon^{2}),$$

1 o 1 10τ o 1 11τ o 1

$$X\ (T\ -\tau,T\ -\varepsilon\tau,\varepsilon)=X\ \ (T\ ,T\ )+\varepsilon X\ \ (T\ ,T\ )+O(\varepsilon^{2}),$$

where the time derivative will takes the values:

. . . .

For obtaining the steady state solution for amplitude and phase, putting $a_1 = \varphi_1 = a_2 = \varphi_2 = 0$ into Eq. (16), the resultant formulas can be solved numerically. To discuss the stability behavior of these solutions, linearizing these equations according to Lyapunov first (indirect) method [20] to give the following system:

where the values of ζ_{mn} ,$(m,\ n = 1,\ 2,3,\ 4)$ are given in "Appendix". Numerically, primary resonance is the worst resonance case that is taken into account in the discussions.

• Results and Discussion

This section provides illustrations of the amplitude and phase system behaviours at different resonance instances. A comparison of time delay and active control is shown, along with the impact of various system settings on the amplitude of the signal.

• Time history

Fig. 3(a, b) shows the time response for the amplitude X_1 , X_2 , where Fig. 3(c) illustrates the system phase plane, Without resonance case and without applying any control system (i.e. $k_1 = k_2 = 0$) at the following parameter variables:

$$\omega = 65,\ \Omega = 100,\ \mu_1 = \mu_2 = 0.5,\ \beta_{11} = -0.003,\ \beta_{13} = -0.82,\ \beta_{14} = 0.55, \beta_{16} = 6.55,$$

$$\beta_5 = 0.9,\ \beta_{22} = -0.82,\ \beta_{21} = -0.001,\ \beta_{24} = 0.5,\ f_o = 7,\ f$$

$= 2, \tau = 0.$

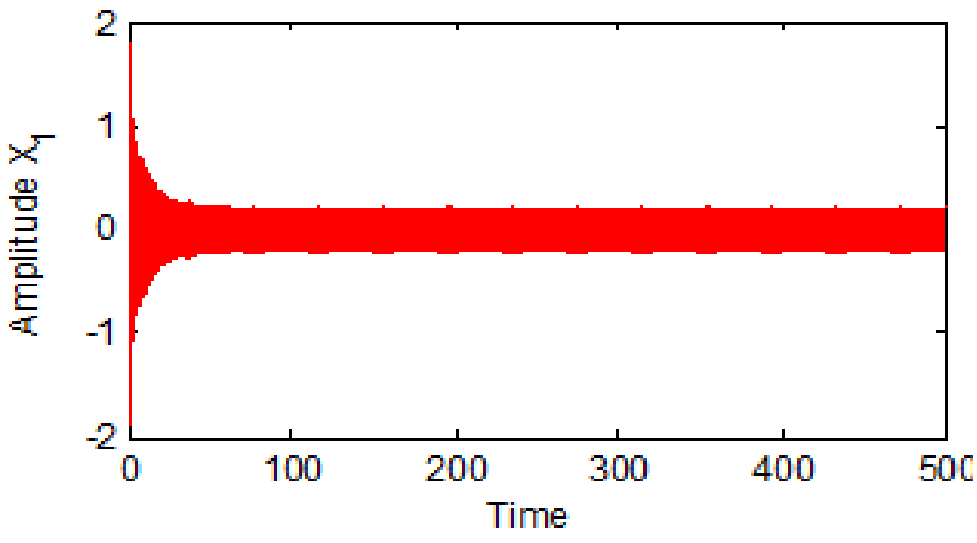

Fig. 3(a). the time response for the amplitude X_1

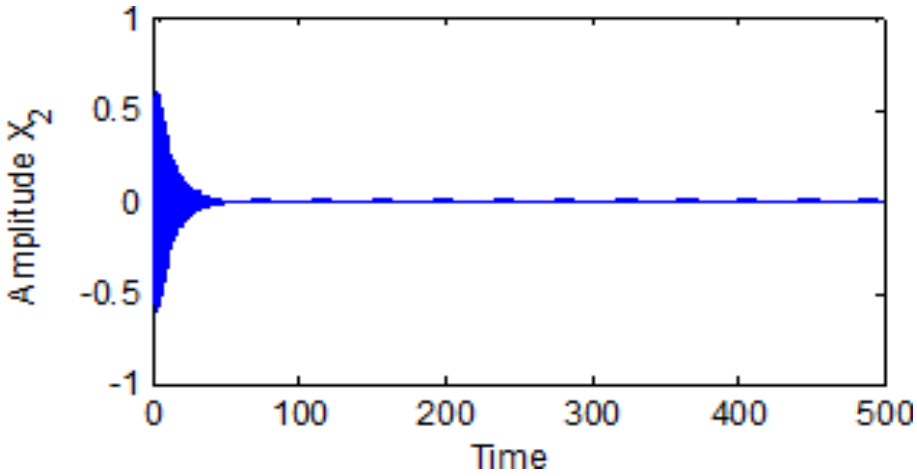

Fig. 3(b). The time response for the amplitude X_1

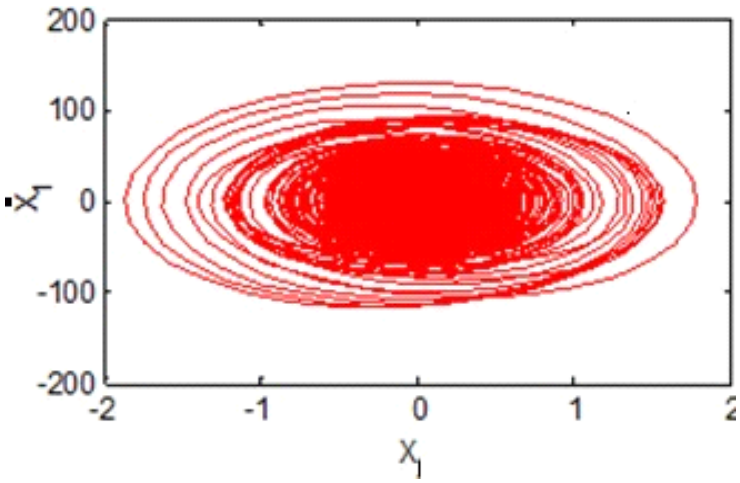

Fig. 3 (c). System phase plane

We can see that the steady state amplitudes are stable in the case of non-resonance operating mode. Fig. 4 clarifies the time history without control and with primary resonance at the same previous parameters except that $\Omega = \omega = 99$, we observe that the amplitudes have been increased due to the resonance operating point.

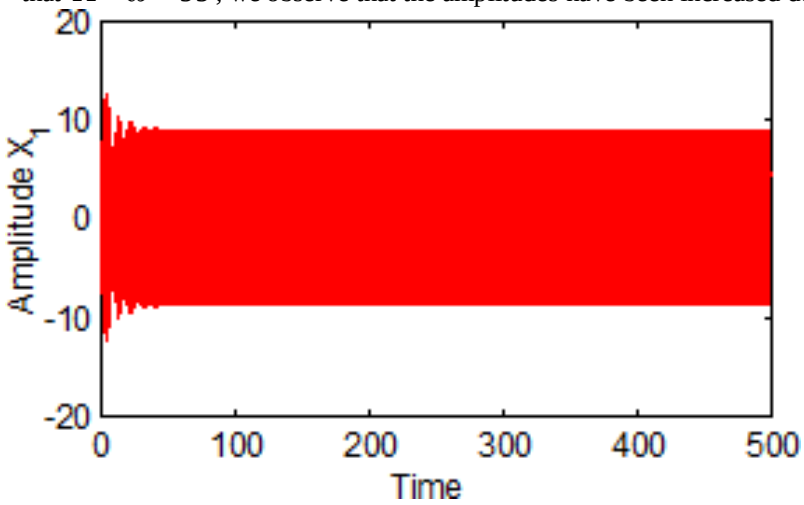

Fig. 4(a). The time response for the amplitude X_1

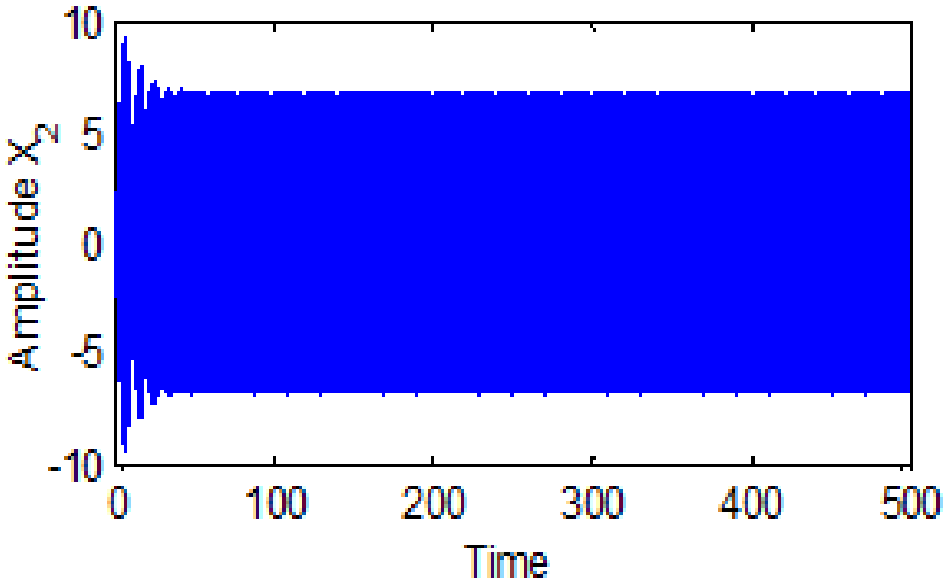

Fig. 4(b). The time response for the amplitude

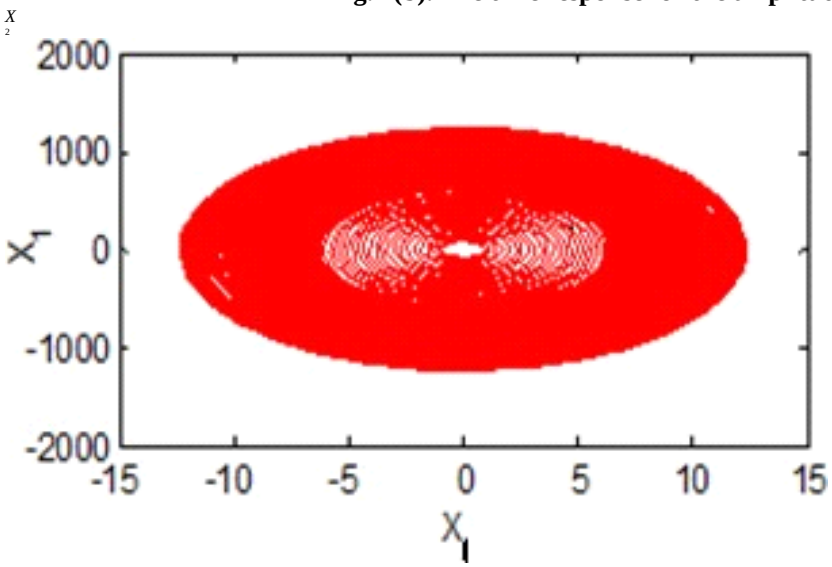

Fig. 4(c). System phase plane

Now applying active and time delay control for the system with primary resonance and comparing the amplitudes. Fig. 5, 6 shows the effect of active and time delay control on both X_1, X_2. We observe that the

effective of active control is about 105%, and Time delay controller is about 125% so the time delay controller is more efficient than active velocity feed-back controller for this system.

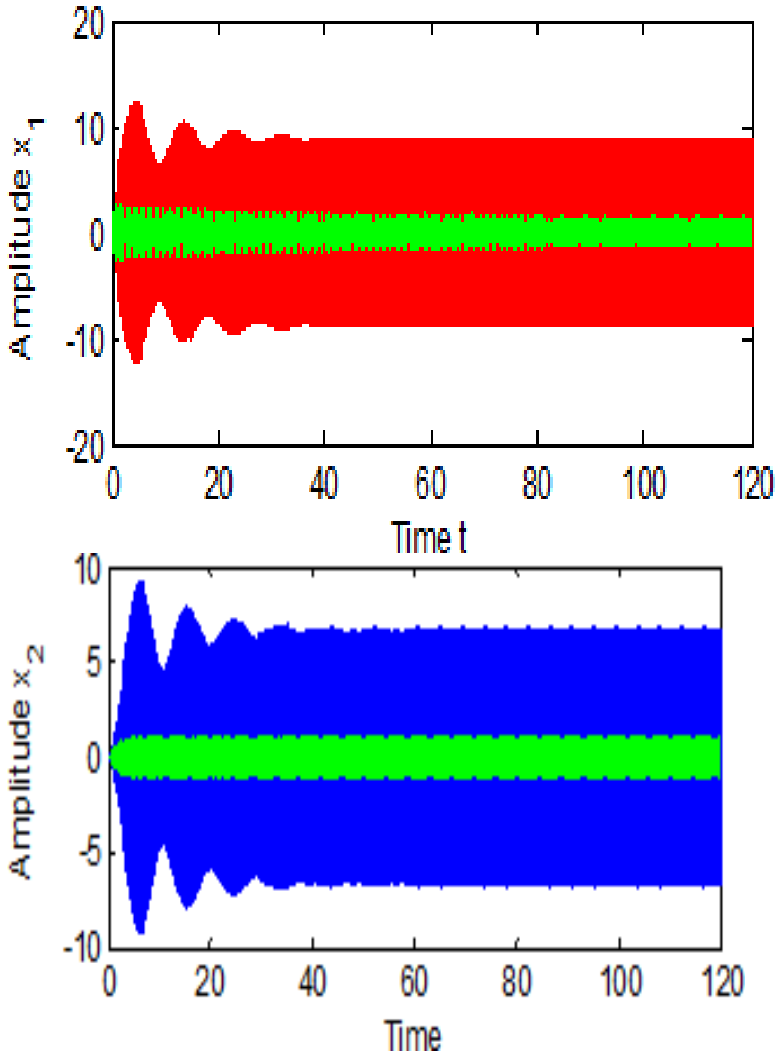

Fig. 5 (a,b). Effect of active control on x_1, x_2 respectively at primary resonance case

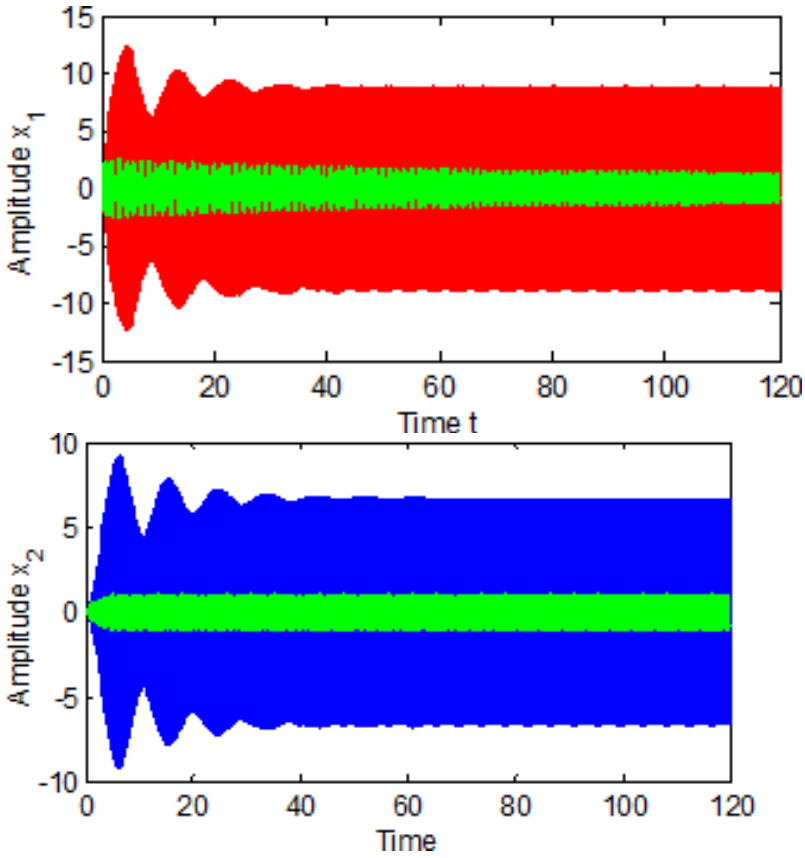

Fig. 6 (a,b). Effect of time delay control on X_1, X_2 respectively at primary resonance case, $\tau = 0.0015$

- **Comparisons with numerical method**

We compared the numerical solution utilising the Rung-Kutta Method (RKM) and the approximate solution caused by (MTSM) in this subsection. In the cases of 0.0015 and 0.0005, respectively, Figures 7 and 8 demonstrate a strong correlation between the numerical results (represented by red curves) and the approximate solution (blue curves).

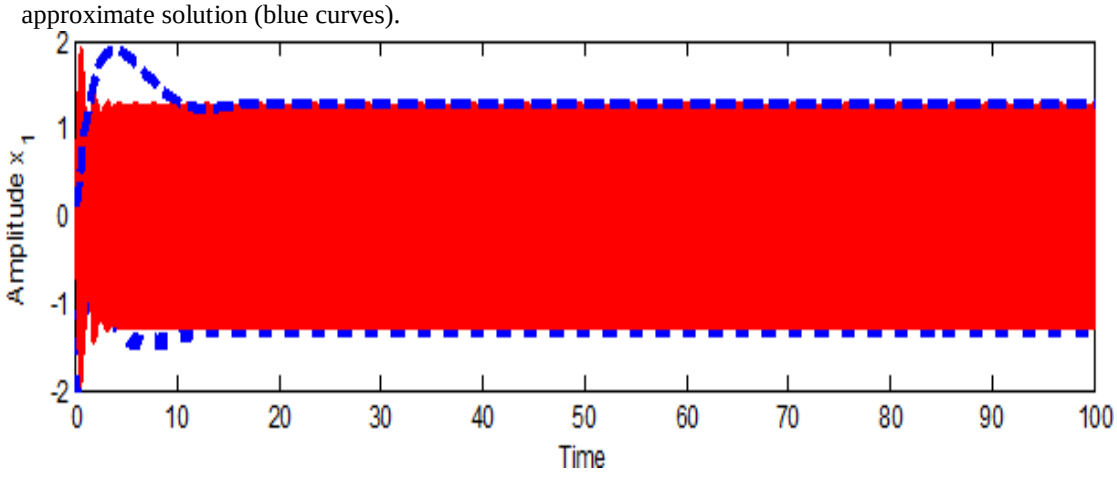

Fig. 7(a). Time history for the amplitude X_1 using MTSM (blue curve) and RKM (red curve)

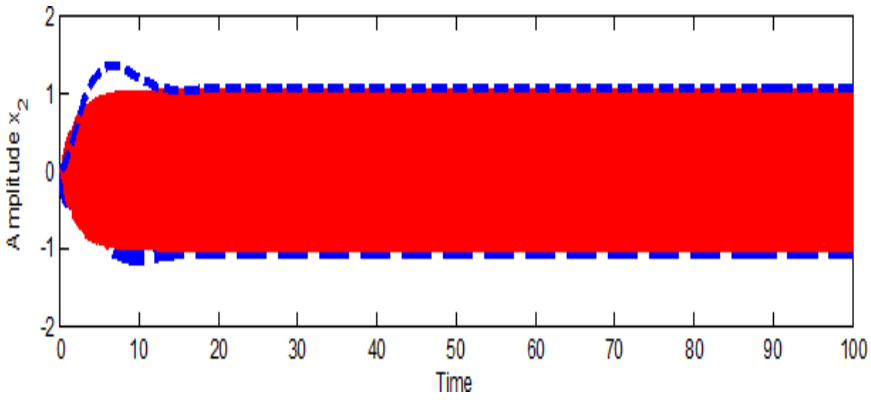

Fig. 7(b). Time history for the amplitude X_2 using RKM (blue curve) and MTSM (red curve)

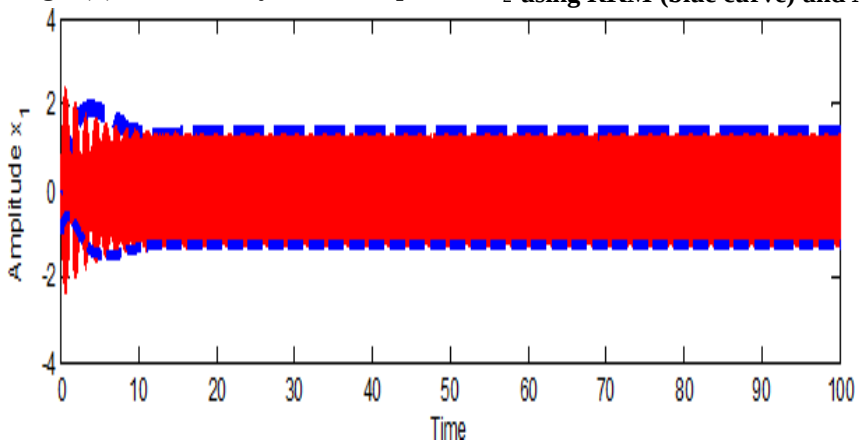

Fig. 8(a). Time history for the amplitude X_1 using MTSM (blue curve) and RKM (red curve) for $\tau = 0.0015$

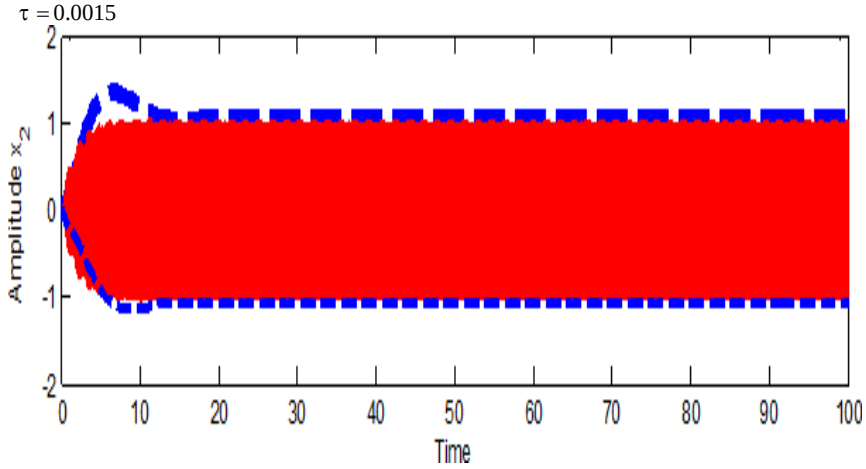

Fig. 8 (b). Time history for the amplitude X_2 using MTSM (blue curve) and RKM (red curve) for $\tau = 0.0015$

- **Frequency response**

Now the following figures show the system amplitude against the detuning parameter σ_1 with change in specified values for system parameters. In Fig. 9 the parameters a_1 ,a_2 with σ_1 in case of primary resonance case with:

$$\omega = \Omega = 100,\ \mu_1 = 0.9, \mu_2 = 0.7,\ \beta_{11} = -0.003,\ \beta_{13} = -0.82,\ \beta_{14} = 0.55, \beta_{16} = 6.55,$$

$$\beta_5 = 0.9, \beta_{22} = -0.82, \beta_{21} = -0.001, \beta_{24} = 0.5, f_o = 7, fk_1 = 1000, k_2 = 0.7, 1, 1.5.$$

$$= 3, \tau = 0.0015, \varepsilon = 0.001,$$

.

We see that when the gain (k 2) increases, the amplitude falls, indicating that the delayed velocity feedback control outperforms the displacement delay. Figures 10 and 11 show how different values of the damping parameters, 1 and α2, as shown in these figures, respectively, affect the amplitude and the influence of A1. The system parameters are set to the same values as those shown in Fig. 9, with k 2 = 1. Figure 10 shows that the values of a1 and a2 are inversely proportional to the damping parameter 1, whereas Figure 11 shows that a1 is

roughly constant with two peaks. This is because it affects the system's second mode's velocity, X 2.

- **Amplitude vs. certain system parameters**

Unless otherwise noted, let's take into consideration the criteria listed in sub-section 3.3. This subsection displays the amplitude range change as the constant and variable rotating forces, f o, f, are varied, as indicated in Fig. 12(a,b), for k 2 = 100, k 2 = 15, and k^ = 90, respectively. Up to maximum amplitude at saturation, the main system's steady state amplitude is a monotonically increasing function of the excitation amplitude. Because of its high value, the saturation value could cause an unstable or damaged system. The behaviour of the amplitude at ‴ ⁉ ⁷ ⁉ 10 is depicted in Figure 13(a, b) with damping parameters 1 and 2, respectively.
It is useful for the system to select a large value for 1, but an expensive material should be used. Therefore, we use suitable materials with appropriate cost and add a specified controller for reducing the amplitude for minimum values in the case of resonance cases. As we can see in Fig. 13, the suitable range for 2 ₣ 0.003 and 1

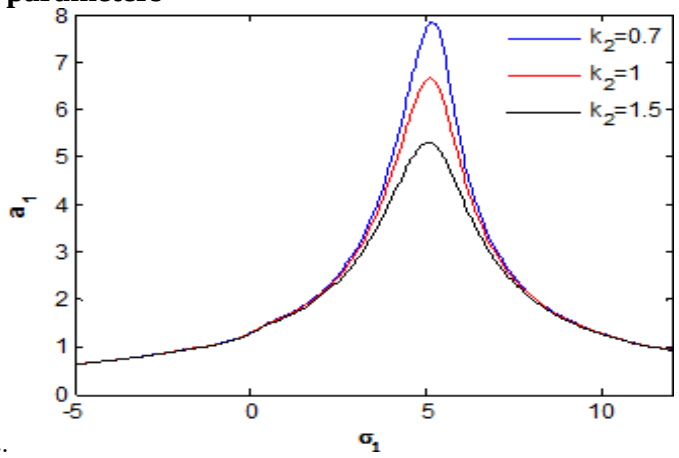

₳ 0.2.

Fig. 9(a). System amplitude a_1 against detuning parameter σ_1 at $k_2 = 0.7,1,1.5$

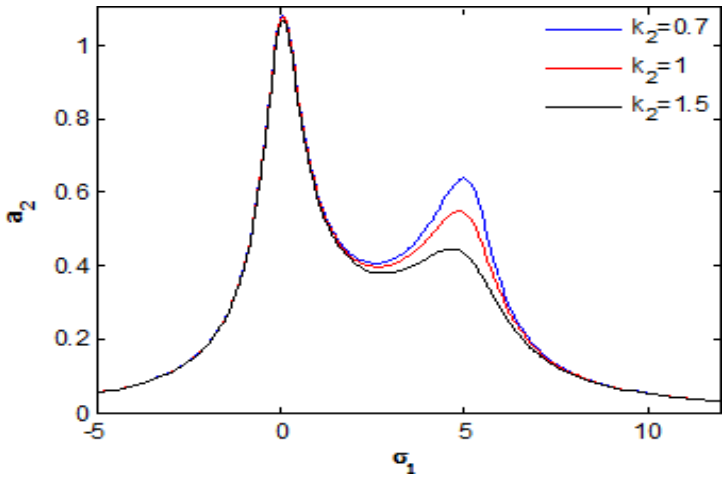

Fig. 9(b). System amplitude a_2 against detuning parameter σ_1 at $k_2 = 0.7, 1, 1.5$

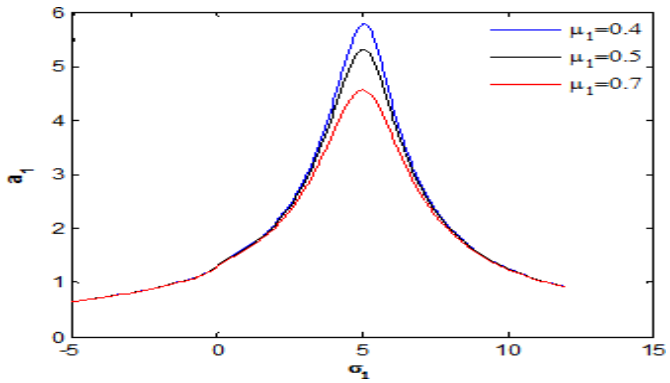

Fig. 10(a). System amplitude a_1 against detuning parameter σ_1 at $\mu_1 = 0.4, 0.5, 0.7$

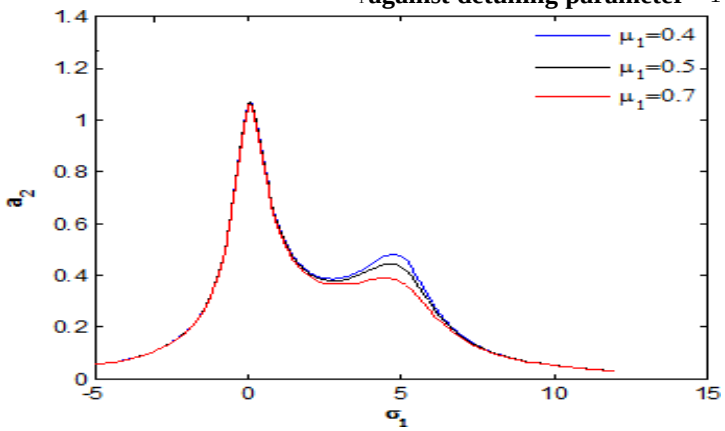

Fig. 10(b). System amplitude a_2 against detuning parameter σ_1 at $\mu_1 = 0.4, 0.5, 0.7$

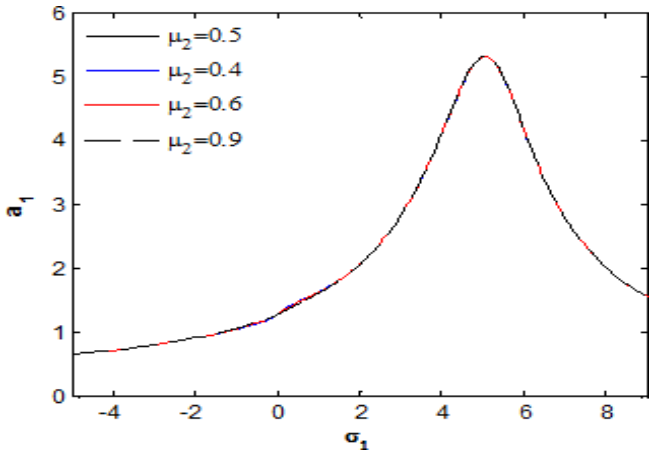

Fig. 11 (a) System amplitude a_1 against detuning parameter σ_1 at $\mu_2 = 0.4,\ 0.5,\ 0.6, 0.9$

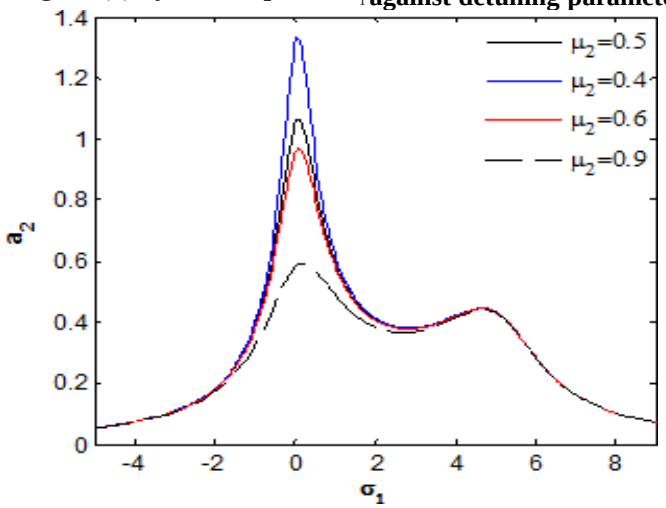

Fig. 11 (b). System amplitude a_2 against detuning parameter σ_1 at $\mu_2 = 0.4,\ 0.5,\ 0.6, 0.9$

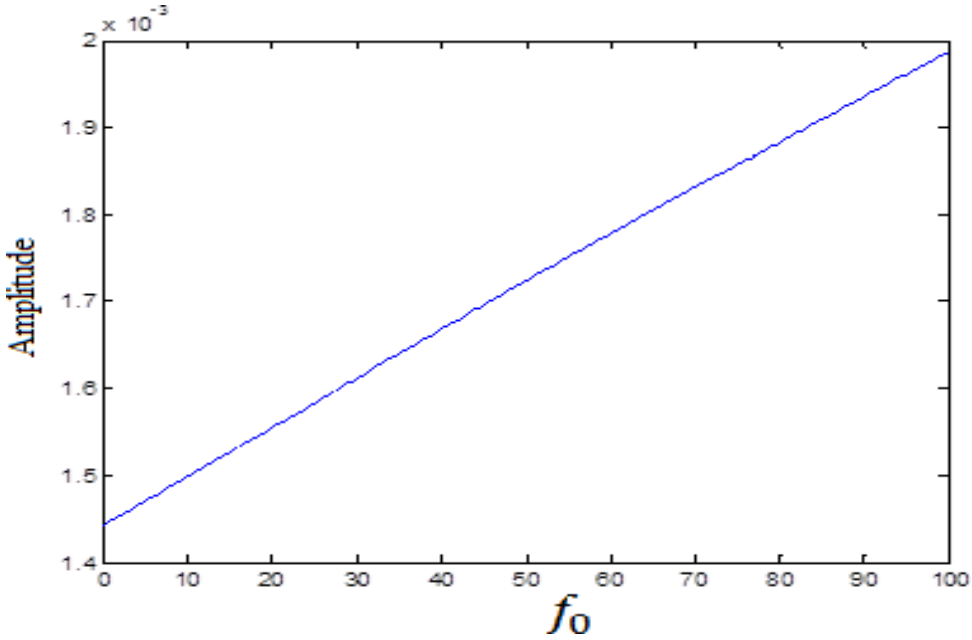

Fig. 12(a). System amplitude against constant rotating forces f_o

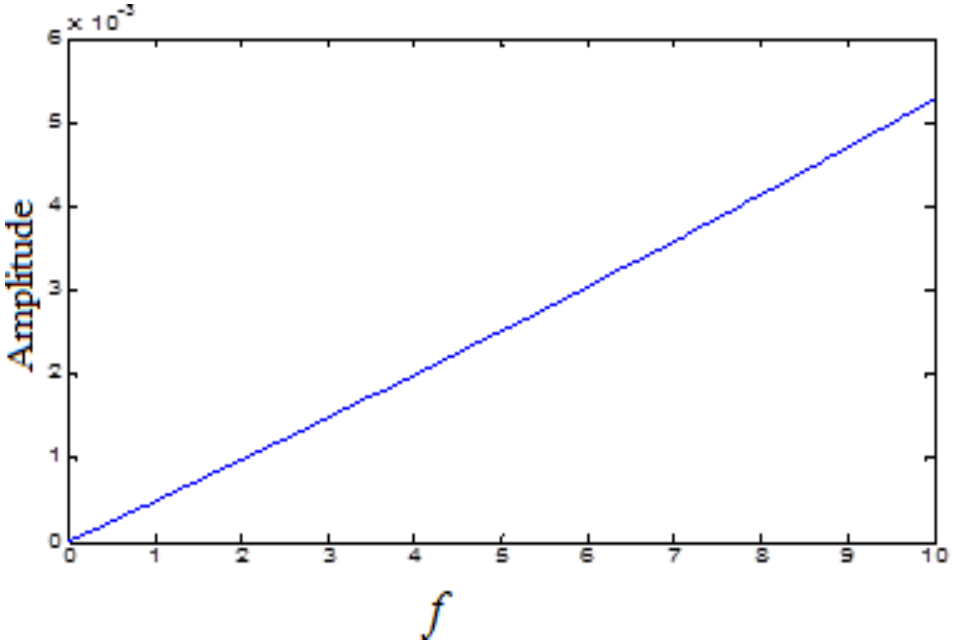

Fig. 12(b). System amplitude against variable rotating forces f

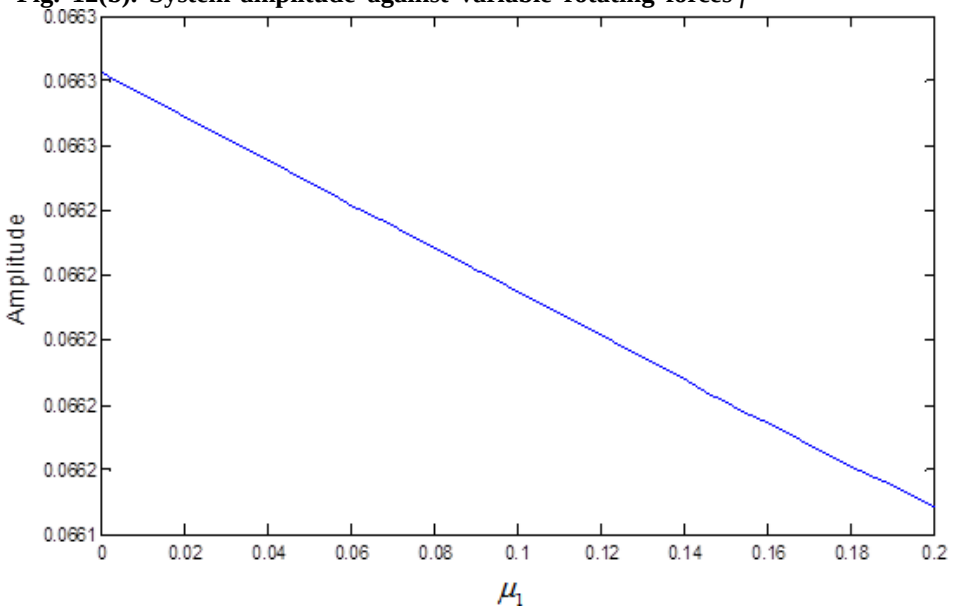

Fig. 13(a). System amplitude against damping parameters μ_1

μ_2

Conclusion

Fig. **13(b). System amplitude against damping parameters** μ_2

This study uses the various time scales approach to analyse a system of nonlinear ordinary differential equations that describe a revolving beam approximately. We investigated how the presence or absence of a time delay affected the displacement feedback system amplitude and velocity. Primary and major parametric resonance, the worst cases of resonance, are studied. We came to the conclusion that the time delay controller is more effective than the active feed-back controller on the velocity for this system. Since the time delay controller's effectiveness is approximately 125% while active control's is approximately 105%, using the time delay controller is advised in this system. To do the stability analysis, the Routh–Hurwiz criteria and the Lyapunov first technique are used. Furthermore, utilising the Rung-Kutta of fourth order method, the approximate solution generated by (MSPT) is compared with the numerical approximation solution. A good agreement between approximate and numerical approaches was provided by the distinction. In order to select the right values for these parameters and achieve system stability, the impacts of the system parameters on the amplitude are examined.

Competing Interests

The authors have stated that there are no conflicting interests.

References

Hardening/softening behaviour and reduced order modelling of nonlinear vibrations of rotating cantilever beams by Thomas O., Sénéchal A, and Deü JF. In 2016 Nonlinear Dyn. 86:1293–1318.

(14) Modal properties of a rotating flexible beam with a concentrated mass based on the absolute nodal coordinate formulation Zhang X, Zhang D, Chen S, Hong J. 2017. Nonlinear Dyn. 88:61–77.

•Aeroelastic analysis of a revolving wind turbine blade using ageometrically accurate formulation, Rezaei MM, Behzad M, Haddadpour H, Moradi H. In 2017 Nonlinear Dyn. 89:2367–2392.

• Arvin H, Bakhtiari-Nejad F. Analysis of a spinning beam using non-linear modes. 2011;46(6):877–897 in Int. J. Non-Linear Mech. Bekhoucha F, Cadou JM, Duigou L, Rechak S. Anisotropic spinning beams subjected to nonlinear forced vibrations. 2013;74(4):1281–1296; Nonlinear Dyn.

Kim H, Chung J. (2016) Nonlinear modelling for rotating cantilever beam dynamic analysis, Nonlinear Dyn. 86:1981–2002.

A coupled-field model featuring an integrated nonlinear piezoelectric active element in a rotating composite beam is presented by Latalski J. (2017) Nonlinear Dyn. 90: 2145–2162.

• Hany El-Gohary and Ali Kandil. Nonlinear Dyn. 2018;91:2631–2649. Examining the efficacy of a time-delayed proportional derivative controller for spinning blade vibrations.

Nonlinear vibrations of a blade with variable rotating speed were studied by Yao MH, Chen YP, and Zhang W in Nonlinear Dyn. 2012;68:487–504.

•Zhang W, Chen YP, Yao MH. Acta Mech. 2014;225:3483–3510: Analysis of nonlinear oscillations and resonant responses of a compressor blade.

– Choi SC, Park JS, Kim JH. PVDF sensors and MFC actuators for active damping of rotating composite thin-walled beams. Compos. Struct. 2006;76:362–374.

Choi SC, Park JS, Kim JH. Piezoelectric fibre composites for vibration control of pre-twisted rotating composite thin-walled beams, J. Sound Vib. 2007;300:176–196.

S Chatterjee, Joy Mondal. International Journal of Non-Linear Mechanics, 2021;131:103684, Controlling self-excited vibration of a nonlinear beam by nonlinear resonant velocity feedback with time-delay.

• Dingguo Zhang, Yongbin Guo, Liang Li, and Wei-Hsin Liao. Journal of Sound and Vibration, 2019;455:46e68; Dynamic modelling and analysis of rotating beams with partially covered enhanced active limited layer damping treatment.

The article "Exponential stabilisation of a non-uniform rotating disk-beam system via a torque control and a finite memory type dynamic boundary control" was published in the Journal of the Franklin Institute in 2019 and was written by Boumediène Chentouf and Nejib Smaoui.

• Lyu LF, Zhu WD. Tracking continuously scanning laser Doppler vibrometer system for operational modal study of a spinning structure under ambient excitation. Mechanical Systems and Signal Processing. 2021;152:107367.
Discontinuous Galerkin approach to massive bending deformation of a bilayer plate with isometry constraint (Andrea Bonito, Ricardo H. Nochetto, and Dimitris Ntogkas), Journal of Computational Physics, 2020; 423:109785.

Mook DT, Nayfeh AH. Nonlinear Oscillations. New York: Wiley, 1995.

YA Amer, AT El-Sayed FO from Darwesh. Asian Research Journal of Mathematics, 2019;12(4):1-17. Active and temporal delay controls on vibrations of the Micro Electro-Mechanical System (MEMS) resonator.
ISSN for article number ARJOM.46389 is 2456-477X.

* Courtney S. Colman, Robert L. Borrelli. John Wiley and Sons, INC., New York, Differential Equation, 1998.

• Gradshteyn IS, Ryzhik LM. Academic Press, San Diego, CA, 6th ed., 2000; 1076.